Ground Penetrating Radar Studies at Mersin University

Caner Özdemir (1), Enes Yiğit (1), and Şevket Demirci (1)

(1) Dept. of Electrical-Electronics Engineering, Mersin University
Çiftlikköy, 33343 Mersin, TURKEY
cozdemir@mersin.edu.tr, enesyigit81@mersin.edu.tr, sdemirci@mersin.edu.tr

Abstract
In this paper, we present the ongoing research on Ground Penetrating Radar (GPR) and the recent studies for imaging buried targets at Mersin University. We have a stepped frequency radar experimental set up to collect real B-scan and C-scan measurements so that we can form 2-D or 3-D GPR images. We have the capability of simulating GPR problems for homogeneous mediums as well. In this paper, we present both simulated and measured GPR images for different buried objects. We further present GPR imaging/focusing algorithms that we developed recently to enhance the quality in GPR images. A variety of measured B-scan GPR images for various buried objects were presented.

1. Introduction

Throughout the centuries, detecting and identifying objects buried under the ground or located interior to a visually opaque medium have been an interesting topic for mankind. Hence, scientists and researchers have put a lot of effort to reach this crucial goal. Many technological approaches from seismic tomography to electromagnetic (EM) radiation techniques have been adopted for different applications from mine detection to archeological excavations [1-5]. Unlike other technologies, GPR uses EM waves ranging from HF to X-band frequencies. A GPR image is constructed by applying signal/image processing techniques to the scattered field data collected by the radar from subsurface environment. A B-scan GPR process is achieved by collecting the EM reflectivity of the subsurface objects when the radar is moving on top of the ground surface and looking downward [1-3]. By applying appropriate signal processing techniques, a 2-D B-scan GPR image can be obtained. To acquire GPR data, either a pulse radar or a stepped frequency radar (SFR) is usually utilized. A small-duration pulse achieving an ultra-wide band (UWB) signal is transmitted for pulse radars [6-8]. However, the scattered energy from the subsurface environment is collected for a finite bandwidth at different frequency points with equal step widths for SFR systems [9].

In this paper, we present the ongoing research and the recent developments for imaging buried targets at Mersin University. We have a SFR experimental set up to collect the real B-scan and C-scan measurements so that we can form 2-D or 3-D GPR images. The main goals of the performed experiments could be summarized as follows: (i) examining different soil properties and corresponding penetration depths at C- and X-band frequencies, (ii) comparing the GPR images for electrically different objects from metals to dielectrics (iii) analyzing the EM reflectivity of those targets, (iv) developing innovative GPR imaging algorithms to be able to clearly display the key scattering mechanisms from the subsurface environment. The paper is organized as follows. In Sect. 2, we present a couple of focusing algorithms to focus 2-D B-scan GPR images. In the next section, we provide some simulation results for imaging buried objects in homogeneous mediums. The GPR images are obtained by both the traditional and the proposed imaging methods. In Sect. 4, we present real GPR images for various buried objects obtained by our SFR experimental set-up. Here, we can easily compare the image intensity levels for electrically different objects. In the last section, some discussions are presented and the work is concluded.

2. GPR focusing algorithms

The common problem in GPR images is the hyperbolic defocusing due to moving radar on top of the ground surface [1-3]. The details of this problem are discussed thoroughly in our previous studies [10-

11] and will not be repeated here. To solve this problem, we have developed a couple of focusing algorithms whose summaries are briefly given below.

2.1 A Hyperbolic Summation Type Focusing Algorithm

This technique is based on the famous Hyperbolic Summation (HS) method that was successfully applied in seismic imaging [11]. The details of this algorithm were presented in [10]. Therefore, we will just briefly remind the steps of this algorithm. (i) As the radar antenna moves along a line while collecting the EM scattering over frequencies, traditional 2-D B-scan GPR image is formed. (ii) For each pixel point; (x_i, z_i) in the 2-D original B-scan GPR image; we calculate the corresponding hyperbolic template using the formula $z = \sqrt{z_i^2 + (X - x_i)^2}$ and trace the pixels under this template. Here *X,* represents the synthetic aperture vector and *z* gives the distance from radar to the point scatterer. (iii) Next, we record the image data for the pixels under this hyperbolic template. (iv) Then, we take the root-mean-square (*rms*) value of the total energy contained in this 1-D complex data under the hyperbolic template as

$$\{rms\ @(x_i,\ z_i)\} = \sqrt{(|E_S|^2 \cdot |E_S^*|^2)/N} = \frac{1}{\sqrt{N}} \sum |E_S|^2 \tag{1}$$

Here, the summation runs over the elements of the energy vector $|E_S|^2$. (v) This calculated *rms* value is recorded in the new GPR image at the location; (x_i, z_i). This process is repeated as all the pixels in the original GPR image are covered.

2.2 A Strip-map SAR based Focusing Algorithm

This technique is mainly motivated by Strip-map Synthetic Aperture Radar (SM-SAR) focusing technique that has been introduced by Soumekh [13] and successfully used in different SAR applications. We adopted this algorithm to GPR applications by improving some features of it. The details of the algorithm were already introduced in [11] and will not be repeated here. We will just highlight the key steps of the method: For a monostatic GPR operation, the captured EM scattering from a point object located at (x_i, z_i) can be written as

$$e(x,t) = \sum_{i=1}^{N} \rho_i X\left[\frac{t - 2\sqrt{z_i^2 + (x_i - x)^2}}{c_m}\right] \tag{2}$$

Here, *X(t)* is the time-domain transmitted signal, ρ_i is the scattering amplitude and c_m is the speed of light in the ground medium. If (2) is transformed to wave number-frequency domain by applying a 2-D Fourier transform (FT) oeration, we get

$$E(k_x, w) = \left(\frac{1}{2\pi}\right) X(w) \frac{e^{-j(\frac{\pi}{4})}}{\sqrt{4k^2 - k_x^2}} \sum_{i=1}^{N} \rho_i e^{-j\sqrt{4k^2 - k_x^2}\cdot z_i - jk_x \cdot x_i} \tag{3}$$

In this equation, $k = w/c_m$ is the wave number and *X(w)* is the FT of the transmitted signal. The amplitude term; $e^{-j(\frac{\pi}{4})} \Big/ \sqrt{4k^2 - k_x^2}$ is ignored since it has no influence on phase. If we think of a 2-D FT of a GPR image of an ideal point scatterer, it should be in the form of

$$G_0(k_x,k_z)=\left(\frac{1}{2\pi}\right)\sum_{i=1}^{N}\rho_i e^{-jk_x x_i - jk_z z_i} \tag{4}$$

Therefore, comparing the results in (3) and (4), and using spatial-frequency transformation equation; $k_z=\sqrt{4k^2-k_x^2}=\sqrt{\frac{4w^2}{c_m^2}-k_x^2}$, we end up $G_0(k_x,k_z)=\frac{E(k_x,w)}{X(w)}$. Then, we get can the 2-D GPR image by taking the 2-D inverse Fourier transform (IFT) of (4) with respect to k_x and k_z as below

$$GPR_{SAR}(x,z)=\frac{1}{2\pi}\int_{-\infty}^{\infty}\int_{-\infty}^{\infty}\frac{E(k_x,k_z)}{X(w)}e^{j(k_x x+k_z z)}dk_x dk_z \tag{5}$$

3. Simulated B-scan GPR images

We test the developed focusing methods for a numerically generated B-scan GPR data obtained by a physical optics (PO) based EM simulator [14] that utilizes the shooting and Bouncing Ray (SBR) technique. This simulator can estimate EM scattering from conducting objects for homogeneous mediums. Therefore; the effect of air-ground interface is ignored assuming that the permittivity of the ground medium is small enough. The EM simulation is carried out by our PO based code assuming that the dielectric constant of the ground is 4. The back-scattered electric field is collected along the synthetic aperture in x ranging from *-0.25m* to *1.25m* for a total of 64 discrete spatial points. The frequency is altered from 6.82 GHz to 9.14 GHz such that the back-scattered signal; S_{11} is collected for a total of 64 discrete frequencies at each spatial point. A pipe, a mine-like cylindrical object and a plate are buried under the ground as their CAD file is viewed as in Fig. 1(a). We first get the GPR image for the B-scan data obtained for these metallic objects as shown in Fig. 1(b). As expected, the image consists of thick hyperbolas centered at the objects' hot spot points. The outlines of the objects are drawn as lines for referencing purposes. After applying proposed focusing algorithms, we got the new focused GPR images as shown in Fig. 1(c) and Fig. 1(d). It is clear that, these images are very well focused and better estimates the location of the dominant scattering points on tops of the buried objects.

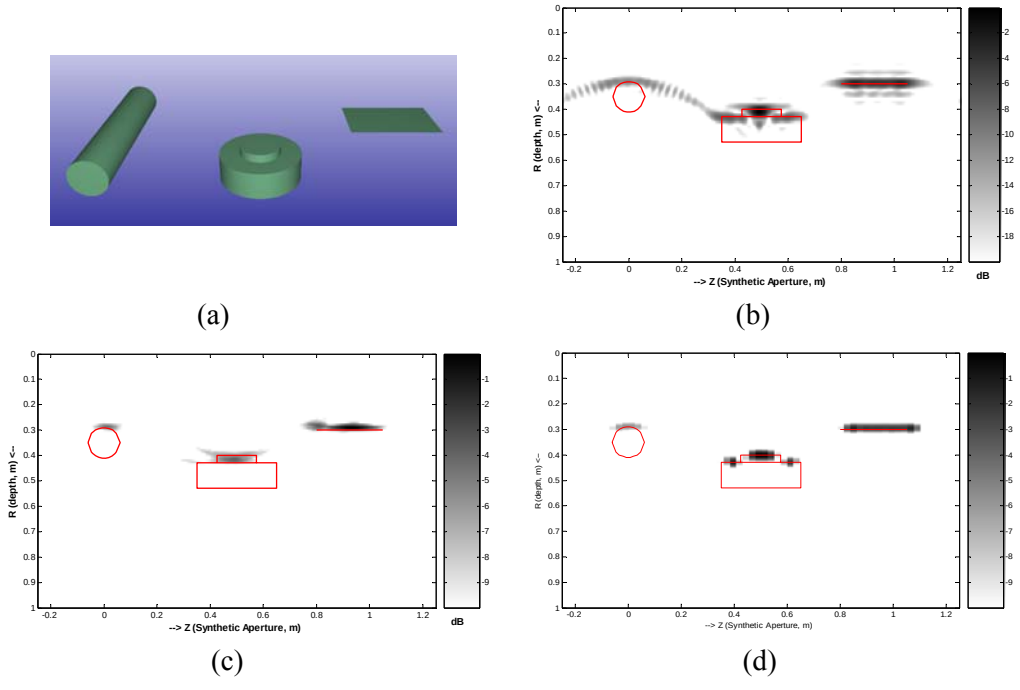

Figure 1. (a) The CAD file of a pipe, a mine-like object and a plate (b) Original defocused GPR image. Focused GPR image after (c) HS based method, (d) SM-SAR based method.

4. Measured B-scan GPR images

The GPR measurements were performed by our SFR experimental set-up whose geometry is shown in Fig. 2. We have constructed a wooden pool that was filled with a dry, homogeneous sand material whose dielectric constant is measured to be constant around 2.4 for C-band frequencies. The measured data was collected via *Agilent E5071B ENA Vector Network Analyzer* (VNA) with the help of C-band pyramidal rectangular horn antennas. The measurements were recorded on a PC thru a GPIB port.

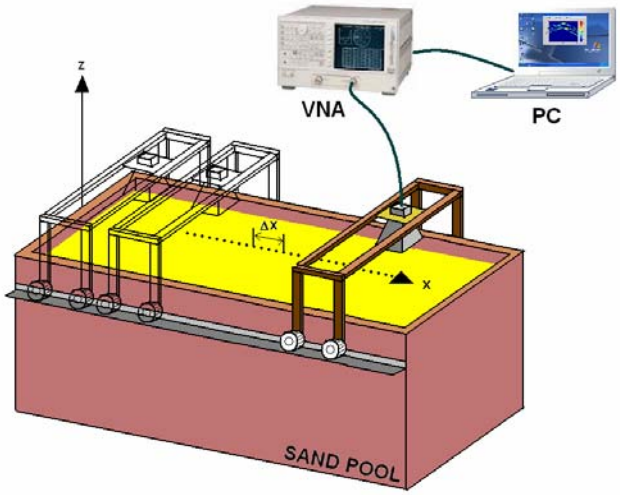

Figure 2. The experimental set-up for collecting B-scan GPR data

In the first experiment, three different objects; a small plastic bottle with full of water, an empty small plastic bottle and a small aluminum plate were buried beneath the surface as shown in Fig. 3(a). The back-scattered data was collected along a synthetic aperture length of *80cm* for a total of 41 discrete spatial points while the frequency was varied from *4.8* to *8.5* GHz with 201 evenly spaced discrete points. The constructed B-scan GPR image is shown in Fig. 3(b) where the dynamic range of the display is set to *35dB*. The reflection from the sand's surface is dominant and easily observed at *z=0cm*. All three objects were successfully imaged with our GPR imaging algorithm. As expected, an intense scattering occurs from the metal object while significant scattering was also collected from water target and air void. Another observation is that the electromagnetic wave can well penetrate sand medium since it is very dry and its permittivity is low. Therefore, we can also detect the scattering from the bottom of the pool at *z=63cm*. As it can be seen from Fig. 3(b), the reflection from sand/ground boundary is visible almost for the entire synthetic aperture.

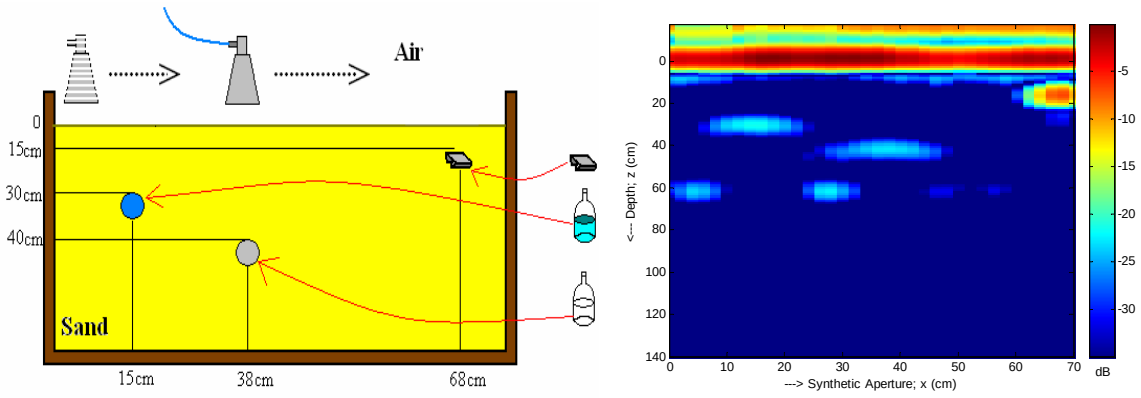

Figure 3. (a) B-scan GPR experimental set up to image different objects (b) B-scan measured GPR images of these buried objects.

As the second experiment, two metal pipes were buried inside the sand. These identical pipes with *6cm* in diameter and *38 cm* in length were buried horizontally at *(x=60cm, z=36cm)* and *(x=80cm, z=25cm)*. This time, a bistatic measurement is taken to mitigate the scattering from the sand's surface. Therefore, two C-band pyramidal rectangular horn antennas were put aside and just above the surface while collecting S_{21} measurements along a straight path of *120cm* with 61 discrete spatial points. For each spatial point, the VNA's frequency is varied from *4.0* to *7.1* GHz with *15.5 MHz* frequency steps to get 201 discrete frequency points. Traditional 2-D B-scan GPR image is attained as depicted in Fig. 4(a) by taking the 1-D IFT of the measured spatial-frequency data. By applying our HS-based focusing algorithm, we obtained the GPR image shown in Fig. 4(b). We also applied our SM-SAR based migration method to focus the image as the result is seen in Fig. 4(c).

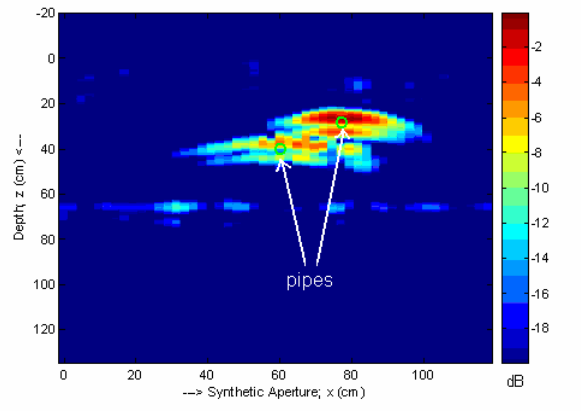

(a)

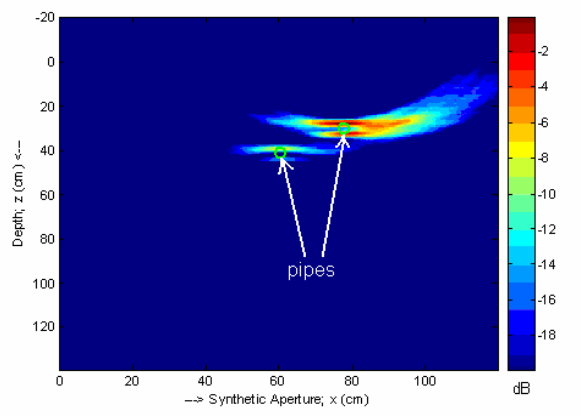

(b)

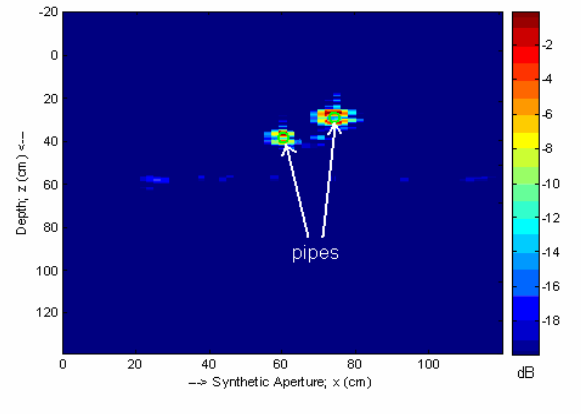

(c)

Figure 4. Measured B-scan GPR images of buried pipes (a) Traditional GPR image. Focused GPR images after applying (b) HS based method, (c) SM-SAR based method.

5. Conclusion

In this paper, we presented recent studies we have conducted on GPR at Mersin University. We presented two different B-scan GPR focusing algorithms that we developed. The formulations of the algorithms were given in Sect. 2. We first demonstrated simulation results for various buried objects. The application of the proposed methods to simulated data yielded very well focused B-scan GPR images. The measured data were collected by our SFR experimental set-up thru various horn antennas with the help of a VNA. Some measurements corresponding to B-scan GPR imagery were presented. The resultant GPR images from these measured data produced good quality GPR images. We could also improve the quality of images by applying our focusing methods to images produced by traditional methods.

Acknowledgements:

This work is supported by the Scientific and Research Council of Turkey (TUBITAK) under grant No. 104E085. The authors are grateful to *Mersin Trakya Cam A.Ş.* for providing sand material and to Department of Mechanical Engineering of Mersin University for providing laboratory facilities for the experiments.

References

[1] D. J. Daniels, *Surface-Penetrating Radar*, London: IEE Press, 1996.

[2] L. Carin, N. Geng, M. McClure, J. Sichina, and L. Nguyen "Ultra-Wide-Band Synthetic-Aperture Radar for Mine-Field Detection" *IEEE Trans. Anten. Propag. Mag.*, vol. 41, no. 1, pp. 18-33, 1999.

[3] L. Jr. Peters, D. J. Daniels and J. D. Young, "Ground penetrating radar as a subsurface environmental sensing tool", *Proc IEEE*, vol. 82, pp. 1802-1822, 1994.

[4] S. Vitebskiy, L. Carin, M. A. Ressler, and F. H. Le, "Ultrawide-band, short pulse ground-penetrating radar: simulation and measurement", *IEEE Trans. Geosci. Remote Sens.,* vol. 35, pp.762-772, 1997.

[5] C. Ozdemir, S. Lim and H. Ling, "A synthetic aperture algorithm for ground-penetrating radar imaging", *Microwave Opt. Tech. Letters*, vol. 42, pp. 412-414. 2004.

[6] L. Carin, N. Geng, M. McClure, J. Sichina, and L. Nguyen, "Ultra-wide-band synthetic- aperture radar for mine-field detection", *IEEE Trans. Anten. Propagat.*, vol. 41, pp. 18-33, 1999.

[7] J. I. Halman, K. A. Shubert and G. T. Ruck, "SAR processing of ground-penetrating radar data for buried UXO detection: results from a surface-based system", *IEEE Trans. Anten. Propagat.*, vol. 46, pp. 1023-1027, 1998.

[8] A. Sullivan, R. Damarla, N. Geng, Y. Dong and L. Carin, "Ultra wide-band synthetic aperture radar for detection of unexploded ordnance: modeling and measurements", *IEEE Trans. Anten. Propagat.*, vol. 48, pp. 1306–1315, 2000.

[9] H. Lee, "Synthetic- Aperture GPR Imaging with Pulse-Echo and Step-Frequency FMCW Systems", *9th International Conference on GPR*, USA, 29 April-3 May 2002, Santa Barbara, CA.

[10] C. Özdemir, Ş. Demirci, E. Yiğit, "A Focusing Method for B-Scan GPR Images ", *11th International Conference on GPR*, 19-22 June 2006, Columbus, OH, USA.

[11] E. Yiğit, C. Özdemir, Ş. Demirci, "Bir Yapay Açıklıklı Radar Tekniği ile Odaklanmış Yere Nüfuz Eden Radar Görüntülerinin Elde Edilmesi", *URSI-TÜRKİYE'2006 Bilimsel Kongresi,* 06-08 Sept. 2006, Ankara, Turkey.

[12] O. Yılmaz, "Seismic data processing", *Society of Exploration Geophysicists*, Tulsa, USA, 1987.

[13] M. Soumekh, *Synthetic Aperture Radar Signal Processing with MATLAB Algorithms*, New York, Wiley, 1999.

[14] H. Ling, R. Chou, and S. W. Lee, "Shooting and bouncing rays: calculation the RCS of an arbitrary shaped cavity", *IEEE Trans. Anten. Propagat.*, vol. 37, pp. 194-205, 1989.